X-ray and NOE Studies on Trinuclear Iridium Hydride Phosphino Oxazoline (PHOX) Complexes

Sebastian P. Smidt and Andreas Pfaltz*

Department of Chemistry, University of Basel, St. Johanns-Ring 19, CH-4056 Basel, Switzerland

Eloísa Martínez-Viviente and Paul S. Pregosin*

Laboratory of Inorganic Chemistry, ETH HCI, Hönggerberg CH-8093 Zürich, Switzerland

Alberto Albinati*

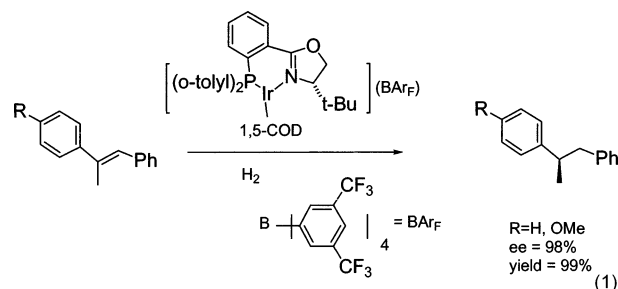*Department of Structural Chemistry (DCSSI), University of Milan, I-20131 Milan, Italy*

Two trinuclear iridium hydride clusters of the type $[Ir_3(\mu_3\text{-}H)(H)_6(PHOX)_3]X_1X_2$ ($X_1 = PF_6$, $X_2 = OTf$; $X_1 = X_2 = PF_6$; $X_1 = X_2 = OTf$; PHOX = (*S*)-4-*tert*-butyl-2-[2-(di-*o*-tolylphosphinyl)-phenyl]-4,5-dihydrooxazole, (*S*)-2-[2-(diphenylphosphinyl)phenyl]-4-isopropyl-4,5-dihydrooxazole) have been prepared and characterized by X-ray diffraction and multidimensional NMR. They contain a single bridging hydride in pseudo-trans position to the P-donors. The complexed PHOX ligands reveal a chiral pocket involving one pseudoequatorial P-aryl substituent and one pseudoaxial (proximate to the oxazoline substituent) P-aryl group. These trinuclear complexes are shown to be inactive as hydrogenation catalysts.
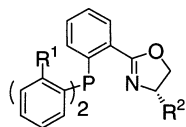
Introduction

Chiral oxazoline complexes of the late transition metals have been recognized as successful enantioselective catalysts in an increasing number of organic transformations,[1] including the Heck and other C−C bond-making reactions,[2] transfer hydrogenation,[3] and hydrosilylation.[4] Most enantioselective hydrogenation reactions are performed with rhodium and ruthenium complexes containing complexed phosphine ligands.[5] Occasionally, an additional ligand is required. Crabtree discovered that complexes of the type $[Ir(1,5\text{-}COD)(PCy_3)(py)]PF_6$ are very active hydrogenation catalysts for tri- and tetrasubstituted olefins.[6] In previous studies,[7,8] the Basel group has reported that the Ir(I) catalyst precursors $[Ir(1,5\text{-}COD)(\mathbf{1})](BAr_F)$, which can be viewed

PHOX ligands

1 $R^1 = CH_3$, $R^2 = $ t-butyl
2 $R^1 = H$, $R^2 = $ i-Pr

as chiral analogues of the Crabtree catalyst, hydrogenate unfunctionalized trisubstituted olefins in methyl-ene chloride solution with excellent enantioselectivity (see eq 1). The lifetime and the activity of this hydro-

R=H, OMe
ee = 98%
yield = 99%
(1)

genation catalyst are known to depend on the nature

(1) For useful overviews, see: (a) Helmchen, G.; Pfaltz, A. *Acc. Chem. Res.* **2000**, *33*, 336−345. (b) Tye, H. *J. Chem. Soc., Perkin Trans. 1* **2000**, 275−298. (c) Ghosh, A. K.; Mathivanan, P.; Cappiello, J. *Tetrahedron: Asymmetry* **1998**, *9*, 1−45.

(2) Helmchen, G. *J. Organomet. Chem.* **1999**, *576*, 203−214.

(3) Nishibayashi, Y.; Takei, I.; Uemura, S.; Hidai, M. *Organometallics* **1999**, *18*, 2291−2293.

(4) (a) Langer, T.; Helmchen, G. *Tetrahedron Lett.* **1996**, *37*, 1381−1384. (b) Nishibayashi, Y.; Takei, I.; Uemura, S.; Hidai, M. *Organometallics* **1998**, *17*, 3420−3422. (c) Nishibayashi, Y.; Segawa, K.; Takada, H.; Ohe, K.; Uemura, S. *Chem. Commun.* **1996**, 847−848. (d) Nishibayashi, Y.; Segawa, K.; Ohe, K.; Uemura, S. *Organometallics* **1995**, *14*, 5486−5487.

(5) (a) Brown, J. M. In *Comprehensive Asymmetric Catalysis*; Jacobsen, E. N., Pfaltz, A., Yamamoto, H., Eds.; Springer: Berlin, 1999; Vol. I, Chapter 5.1, pp 121−182. (b) Noyori, R. *Angew. Chem., Int. Ed.* **2002**, *41*, 2008−2022. (c) Knowles, W. S. *Angew. Chem., Int. Ed.* **2002**, *41*, 1998−2007.

(6) Crabtree, R. H. *Acc. Chem. Res.* **1979**, *12*, 331−338.

(7) (a) Lightfoot, A.; Schnider, P.; Pfaltz, A. *Angew. Chem., Int. Ed.* **1998**, *37*, 2897−2899. (b) Blackmond, D. G.; Lightfoot, A.; Pfaltz, A.; Rosner, T.; Schnider, P.; Zimmermann, N. *Chirality* **2000**, *12*, 442−449. (c) Cozzi, P. G.; Zimmermann, N.; Hilgraf, R.; Schaffner, S.; Pfaltz, A. *Adv. Synth. Catal.* **2001**, *343*, 450−454. (d) Blankenstein, J.; Pfaltz, A. *Angew. Chem., Int. Ed.* **2001**, *40*, 4445−4447. (e) Menges, F.; Pfaltz, A. *Adv. Synth. Catal.* **2002**, *344*, 40−44. (f) Pfaltz, A.; Blankenstein, J.; Hilgraf, R.; Hörmann, E.; McIntyre, S.; Menges, F.; Schönleber, M.; Smidt, S. P.; Wüstenberg, B.; Zimmermann, N. *Adv. Synth. Catal.*, in press.

(8) Imine hydrogenation: (a) Schnider, P.; Koch, G.; Prétôt, R.; Wang, G.; Bohnen, F. M.; Krüger, C.; Pfaltz, A. *Chem. Eur. J.* **1997**, *3*, 887−892. (b) Kainz, S.; Brinkmann, A.; Leitner, W.; Pfaltz, A. *J. Am. Chem. Soc.* **1999**, *121*, 6421−6429.
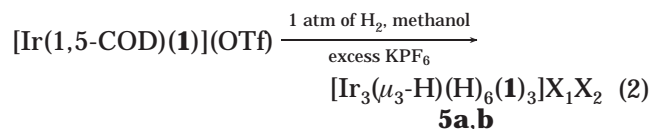
of the anion: the catalyst with PF_6^- as the anion has a rather shorter lifetime than the analogous BAr_F^- derivative.[9] After the catalytic hydrogenation reactions, an NMR spectroscopic analysis of the remaining iridium species in solution suggested the formation of a trimeric iridium hydrido complex,[10] in analogy with the findings by Crabtree.[11] However, a structurally defined compound could not be isolated at that time. Recently,[9] after catalytic hydrogenation of *trans*-α-methylstilbene under standard conditions with the corresponding PF_6^- and BAr_F^- complexes, a trimeric hydride species has been identified as a product by NMR and electrospray MS after full conversion of the alkene. Interestingly, with the BAr_F^- complex, the iridium trimer is formed only as a minor product in methylene chloride, whereas the PF_6^- salt shows a much stronger tendency for trimer formation.

The question of loss of activity in Ir-based hydrogenation chemistry has been addressed previously. It is known that mononuclear iridium complexes, e.g. [Ir(1,5-COD)(P,N ligand types)](anion), react under hydrogen in solution to afford small hydrido-cluster complexes. Crabtree and co-workers[11] and Pignolet and co-workers[12] have reported preparative, NMR, and X-ray diffraction studies for the cationic species [$Ir_3(\mu_3$-H)H$_6$-(pyridine)$_3$(PCy$_3$)$_3$](PF$_6$)$_2$ (**3**) and [$Ir_3(\mu_3$-H)H$_6$(PN)$_3$](BF$_4$)$_2$ (**4**; PN = 1-(2-pyridyl)-2-(diphenylphosphino)ethane), respectively. These trinuclear bridging hydride complexes contain three "IrH$_2$(pyridine)(PCy$_3$)" and three "IrH$_2$(PN)" units, respectively, held together by Ir−Ir metal bonds and the triply bridging hydride. These clusters are thought not to be catalytically active in hydrogenation chemistry. There is little known about the formation of these clusters as a function of counterion so that, possibly, the inactive bridging hydride species are formed at different rates for the different anions.
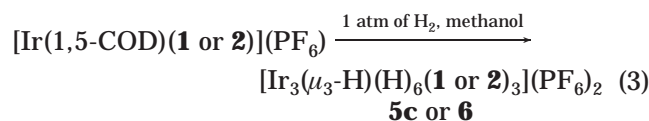
We report here the first isolation and full characterization of two Ir−PHOX cationic complexes of the type [$Ir_3(\mu_3$-H)(H)$_6$(**1** or **2**)$_3$]$^{2+}$ (**5a** and **6**), derived from our enantioselective hydrogenation catalysts [Ir(1,5-COD)(PHOX)]PF$_6$. Further, we show that these iridium clusters do not possess any catalytic activity for the hydrogenation of alkenes, although they have interesting solution and solid-state structures.

Results and Discussion

Solid-State Structures of 5a and 6. The new trinuclear hydride complexes could be prepared in good yield, as shown in eqs 2 and 3 as well as in the Experimental Section. Using the triflate as starting

$$[Ir(1,5\text{-}COD)(\mathbf{1})](OTf) \xrightarrow[\text{excess KPF}_6]{1 \text{ atm of H}_2, \text{ methanol}} [Ir_3(\mu_3\text{-H})(H)_6(\mathbf{1})_3]X_1X_2 \quad (2)$$
$$\mathbf{5a,b}$$

5a, X$_1$ = PF$_6$, X$_2$ = OTf; **5b**, X$_1$ = X$_2$ = OTf

$$[Ir(1,5\text{-}COD)(\mathbf{1 \text{ or } 2})](PF_6) \xrightarrow{1 \text{ atm of H}_2, \text{ methanol}} [Ir_3(\mu_3\text{-H})(H)_6(\mathbf{1 \text{ or } 2})_3](PF_6)_2 \quad (3)$$
$$\mathbf{5c \text{ or } 6}$$

material in the presence of KPF$_6$ afforded a mixed salt, **5a**, which eventually provided crystals suitable for X-ray

Table 1. Selected Distances (Å) and Angles (deg) for 5a and 6

atoms	5a	6
Ir(1)−N(1)	2.132(10)	2.063(7)
Ir(2)−N(2)	2.121(9)	2.107(7)
Ir(3)−N(3)	2.124(10)	2.088(7)
Ir(1)−P(1)	2.234(3)	2.187(2)
Ir(2)−P(2)	2.230(3)	2.210(2)
Ir(3)−P(3)	2.238(3)	2.223(2)
Ir(1)−Ir(3)	2.742(1)	2.7130(4)
Ir(1)−Ir(2)	2.749(1)	2.7089(4)
Ir(2)−Ir(3)	2.739(1)	2.7108(4)
Ir(1)−HB	1.93(9)	n.d.
Ir(2)−HB	2.05(10)	n.d.
Ir(3)−HB	2.26(9)	n.d.
P−C[a]	1.84(1)	1.83(1)
N(1)−C(11)	1.28(1)	1.286(12)
N(1)−C(13)	1.50(1)	1.508(14)
O(1)−C(11)	1.33(1)	1.337(11)
O(1)−C(12)	1.45(1)	1.447(17)
N(1)−Ir(1)−P(1)	84.6(3)	87.2(2)
N(2)−Ir(2)−P(2)	85.2(3)	85.9(2)
N(3)−Ir(3)−P(3)	84.5(2)	84.9(2)
Ir(3)−Ir(2)−Ir(1)	59.95(2)	59.93(1)
Ir(3)−Ir(1)−Ir(2)	59.84(2)	60.00(1)
Ir(2)−Ir(3)−Ir(1)	60.21(3)	60.08(1)
N(1)−Ir(1)−Ir(3)	91.6(3)	94.2(2)
N(1)−Ir(1)−Ir(2)	141.0(2)	141.6(2)
N(2)−Ir(2)−Ir(1)	92.5(3)	92.58(19)
N(2)−Ir(2)−Ir(3)	140.3(3)	136.2(2)
N(3)−Ir(3)−Ir(2)	92.8(2)	91.2(2)
N(3)−Ir(3)−Ir(1)	140.8(2)	142.5(2)
P(2)−Ir(2)−Ir(1)	132.99(8)	126.80(6)
P(2)−Ir(2)−Ir(3)	134.40(7)	138.62(7)
P(1)−Ir(1)−Ir(3)	134.54(8)	134.18(6)
P(1)−Ir(1)−Ir(2)	134.19(8)	131.20(6)
P(3)−Ir(3)−Ir(2)	132.89(8)	131.59(6)
P(3)−Ir(3)−Ir(1)	134.58(8)	139.94(6)

[a] Average value.

diffraction. The more conventional bis(triflate) **5b** (formed by omitting the addition of KPF$_6$) was also prepared. Compounds **5c** and **6** could be conveniently prepared from the PF_6^- precursors. The solid-state structures for **5a** and **6** were determined by X-ray diffraction methods, and Table 1 shows a list of selected bond angles and bond distances for both clusters. Views of the cations are shown in parts a and b of Figure 1.

Toward the end of the refinement for **5a** the Fourier difference map showed a peak in a position consistent with the presence of a triply bridging hydride. This hydride position was refined in the final least-squares cycles, without constraints, using an isotropic temperature factor. The relatively high standard deviation associated with the hydride position prevents a detailed discussion of the nature of the bridge. As shown in Figure 2, HB lies above the plane defined by the three Ir atoms, in positions pseudo-trans to the three terminal P atoms, on average ca. 2 Å from the three metals. The average of the three P−Ir−HB angles is ca. 174°. The six terminal hydride ligands for **5a** and **6** could not be located, although their relative positions could be inferred from the observed coordination sphere.

(9) Smidt, S. P.; Zimmermann, N.; Studer, M.; Pfaltz, A. Manuscript in preparation.
(10) Schnider, P. Ph.D. Dissertation, University of Basel, 1996.
(11) Chodosh, D. F.; Crabtree, R. H.; Felkin, H.; Morris, G. E. *J. Organomet. Chem.* **1978**, *161*, C67−C70.
(12) (a) Wang, H.; Casalnuovo, A. L.; Johnson, B. J.; Mueting, A. M.; Pignolet, L. H. *Inorg. Chem.* **1988**, *27*, 325−331. (b) Wang, H. H.; Pignolet, L. H. *Inorg. Chem.* **1980**, *19*, 1470.
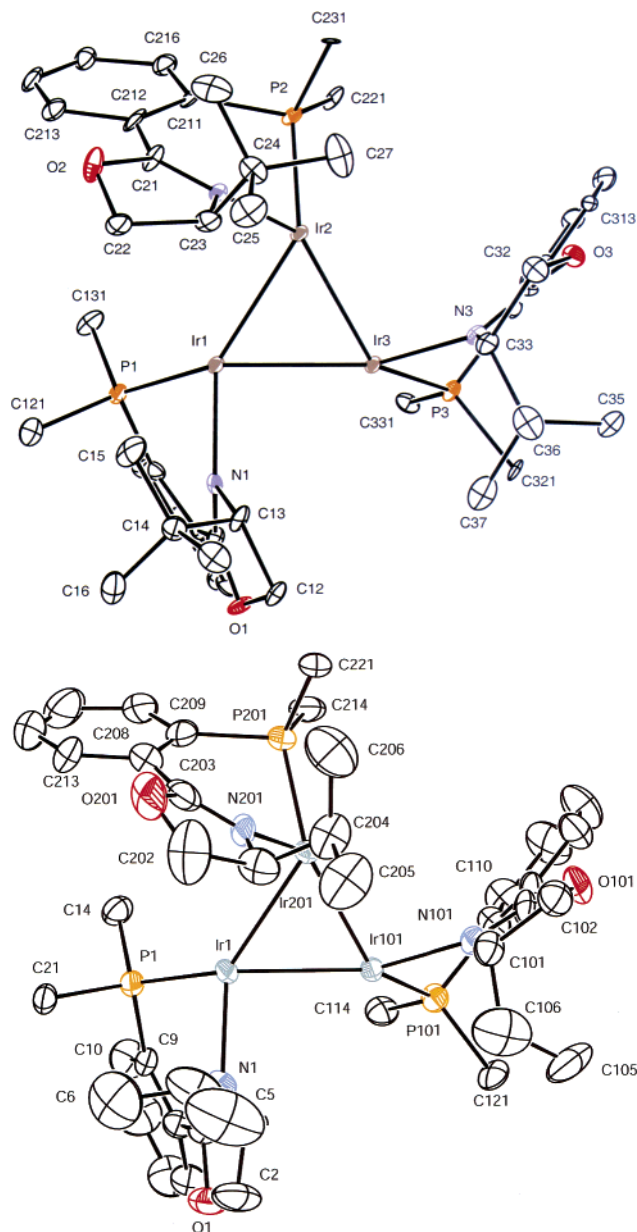
Figure 1. ORTEP views of (a, top) **5a** and (b, bottom) **6**. Ellipsoids are drawn at 30% probability, anions and hydrogen atoms are omitted, and only the ipso C atoms of the P-aryl groups are drawn for reasons of clarity and space. For structure **6**, a different numbering scheme was used: Ir(2) equals Ir(201), Ir(3) equals Ir(101), etc.

The oxazoline substituents (*tert*-butyl in **5a** and isopropyl in **6**) and the bridging hydride both lie on the same side of the plane defined by the three metal atoms.

The three six-membered chelate rings in **5a** and **6** are strongly puckered. If one defines a coordination plane as consisting of the P, N, and Ir atoms, then the three sp^2 carbons of the chelate ring (e.g., C11, C111, and C112 from the chelate ring with Ir1 in **5a**) are all ca. 0.8−1.6 Å removed from this plane (see Figure 3). This figure, which shows only one of the three Ir−(PN) units in **5a**, also indicates that one of the two P(*o*-tolyl) rings is pseudoaxial and proximate to the *tert*-butyl group, a feature that will be emphasized in the solution discussion.

The three Ir atoms make an approximate equilateral triangle with Ir−Ir−Ir angles close to 60°. The averages
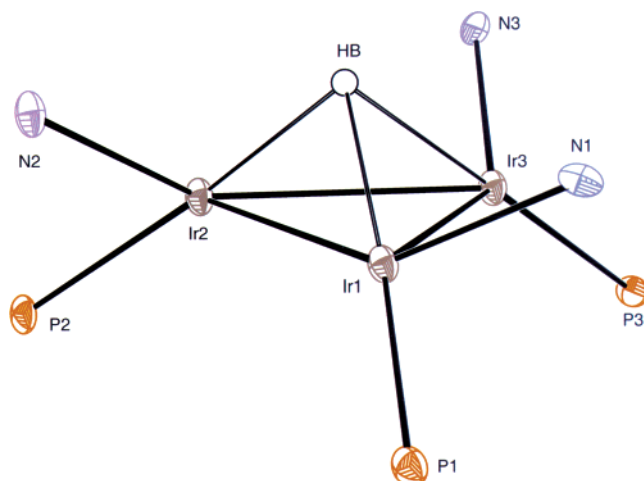

Figure 2. View of the relative position of the bridging hydride HB in **5a**.

of the Ir−Ir, Ir−P and Ir−N bond distances, ca. 2.74, 2.23, and 2.13 Å, respectively, are in good agreement with those observed for the two trinuclear literature examples, **3** and **4**, noted above,[11,12] and a comparison of these and other values is given in Table 2. A search of the crystallographic literature[13] on Ir$_3$ clusters reveals a median value for the Ir−Ir bond distance distribution of ca. 2.745 Å, suggesting that our observed values are normal. In Table 2, there are crystallographically significant differences between the Ir−Ir, Ir−P, and Ir−N bond distances for **5a** and **6**, with the former revealing slightly longer values. These differences might be attributed to the different steric demands of **1** and **2**. However, comparison of space-filling models for **5a** and **6** do not indicate any special strain. The values of the PN chelate bite angle, at 84.8° for **5a** and at 86.0° for **6**, are comparable to those found for the precursor complexes [Ir(1,5-COD)(**1** or **2**)]PF$_6$ (85.6 and 85.9° P−Ir−N angles, respectively).[8a,14]

Differences between the two structures are best seen in Figure 4, which shows a partial superposition of the X-ray crystal structures of **5a** and **6**. Although the structures are very similar, the aromatic substituents on the phosphorus atoms of the two ligands are somewhat displaced and rotated with respect to one another.

The anions come quite close to the cationic species in the solid state. In **5a**, a close contact of ca. 2.46 Å is found between an F atom of the PF$_6^-$ anion and the aromatic H para to the oxazoline moiety and another contact of ca. 2.85 Å between an O atom of the triflate to the same H atom of another aryl ring. In **6**, these contacts are rather different in that one PF$_6^-$ anion shows a close contact of ca. 2.58 Å from an F atom to the oxazoline CH$_2$ group. The second PF$_6^-$ anion shows a contact of ca. 3.40 Å from an F atom to one isopropyl methyl group.

Solution Structure for the Trinuclear Iridium Complex 5a. Complex **5a** reveals three hydride ^{1}H resonances at relatively low frequency, δ −7.07, −17.84, and −21.32, plus a singlet in the ^{31}P spec-

(13) A histogram of Ir−Ir bond lengths was derived with VISTA, version 2.1 with data taken from 141 iridium clusters containing at least one Ir$_3$ triangle in the Cambridge Crystallographic Database.
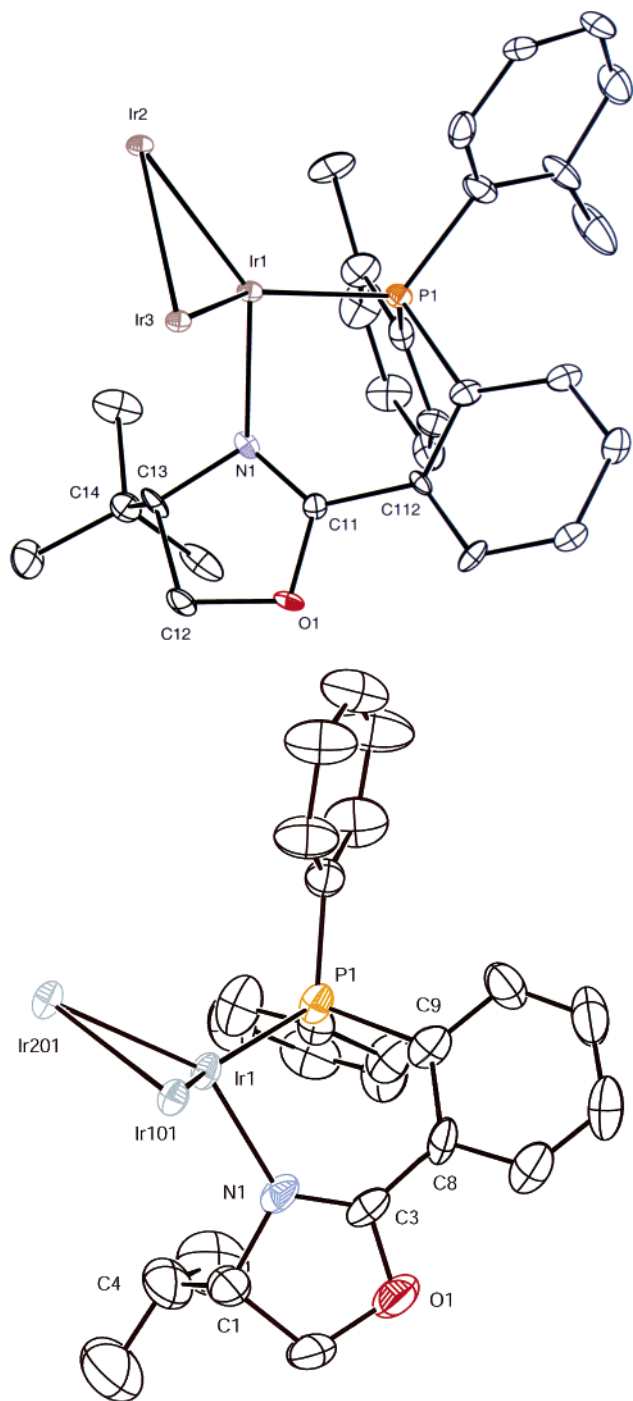(14) Smidt, S. P.; Mukherjee, P.; Neuburger, M.; Pfaltz, A. Unpublished results.

Figure 3. Views of (a) one of the three PN ligands complexed in **5a** and (b) one of the three P,N ligands complexed in **6**. Hydrogen atoms are omitted.

Table 2. Average Distances (Å) and Angles (deg) in Four Trinuclear Compounds[a]

	3	4	5a	6
Ir−Ir	2.765(1)	2.746(1)	2.743(5)	2.711(2)
Ir−P	2.286(3)	2.217(3)	2.234(4)	2.21(2)
Ir−N	2.139(8)	2.115(8)	2.126(6)	2.09(2)
P−Ir−N	95.8(2)	93.7(2)	84.8(3)	86.0(11)

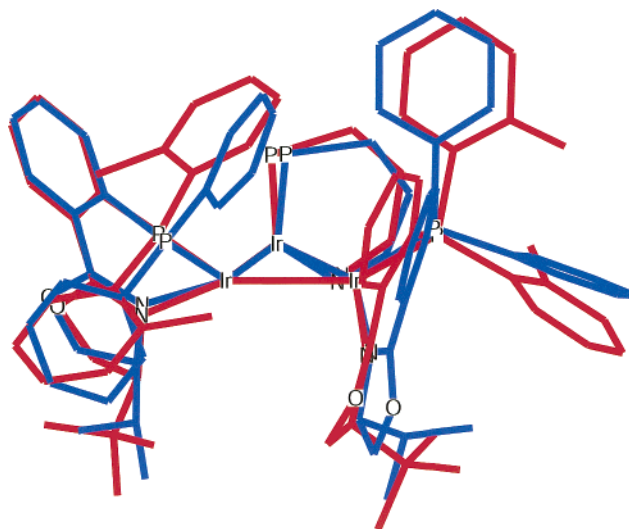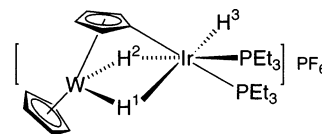[a] Standard deviations on the mean are given in parentheses: $\sigma = (1/(n-1)\sum_i(\bar{x} - x_i)^2)^{1/2}$.

Figure 4. Superposition of sections of the solid-state structures of **5a** (red) and **6** (blue), using Chem 3D.

$^2J(^{31}P,^1H)_{trans}$ value is reported to be 65–70 Hz.[12b,17a]

Further, in the dinuclear tungsten–iridium complex[17b] shown, the observed $^2J(^{31}P,^1H)_{trans}$ value is reported to be 47.6 Hz: i.e., almost identical with the observed values for **5a** and **6**. Moreover, the analogous $^2J(^{31}P,^1H)_{trans}$ coupling constants in complexes **3** and **4** are very close to those found for **5a** and **6**. It would seem that changing the nature of the hydride bonding from terminal to bridging is sufficient to drastically reduce $^2J(^{31}P,^1H)_{trans}$.

The conformation of complexed **1** in solution for **5a** was determined using a variety of one- and two-dimensional NMR methods. Figure 5 shows the $^{31}P,^1H$ correlation for **5a**. There are three cross-peaks in the hydride region (Figure 5a), arising from $^2J(^{31}P,^1H)$ interactions, and two further strong cross-peaks in the aromatic region, stemming from $^3J(^{31}P,^1H)$ (Figure 5b). There are additional weaker cross-peaks in the aromatic region due to four-bond and longer P,H spin−spin interactions. Specifically, the low-frequency strong cross-peak in the aromatic region at ca. δ 6.85 arises from two overlapping

trum at δ 8.25. The μ_3-hydride signal at δ −7.07 appears as a quartet, $^2J(^{31}P,^1H) = 46$ Hz, due to the three equivalent ^{31}P spins. Given the solid-state structure, it is reasonable that the three equivalent P atoms trans to the bridging hydride ligand afford a fairly large $^2J(^{31}P,^1H)$ value, whereas the remaining $^2J(^{31}P,^1H)$ values are relatively small. Nevertheless, this $^2J(^{31}P,^1H)$ value is modest in that typical values of $^2J(^{31}P,^1H)_{trans}$ in mononuclear complexes are on the order of 120−160 Hz.[15,16] In the dinuclear iridium complexes $[Ir_2(\mu_2\text{-H})_3(H)_2(PP)_2]X$, in which there is μ_2 (and not μ_3) hydride bonding, the observed

(15) Parish, R. V. *NMR, NQR, EPR and Mössbauer Spectroscopy in Inorganic Chemistry*; Ellis Horwood: New York, 1990.
(16) Jesson, J. P. In *Transition Metal Hydrides*; Muetterties, E. L., Ed.; Marcel Dekker: New York, 1971; pp 75−201.
(17) (a) Crabtree, R. H.; Felkin, H.; Morris, G. E.; King, T. J.; Richards, J. A. *J. Organomet. Chem.* **1976**, *113*, C7−C9. (b) Pregosin, P. S.; Togni, A. T.; Venanzi, L. M. *Angew. Chem., Int. Ed. Engl.* **1981**, *20*, 668−669.
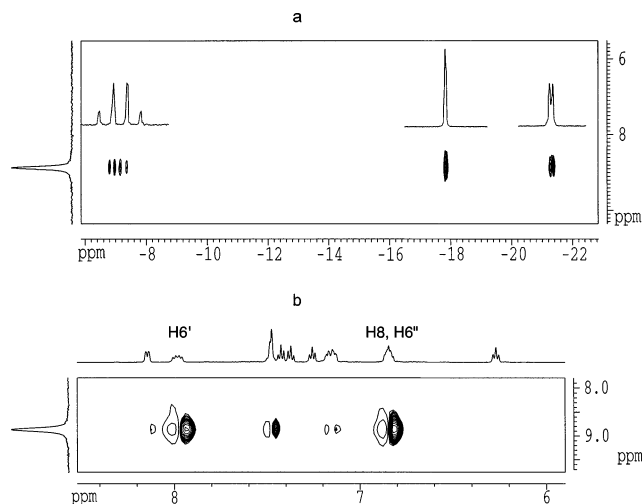
Figure 5. Section of the ^{31}P,^{1}H correlation for **5** showing (a, top) the three hydride ligands and (b, bottom) the three aromatic protons in positions ortho to the P atom. The signal at δ 6.85 arises from two overlapping nonequivalent ortho protons.

nonequivalent ortho protons, H8 and H6″. The second strong cross-peak at ca. δ 7.98 stems from the ortho proton H6′ of the second P-*o*-tolyl fragment. These three protons are indicated in the fragment **A**.
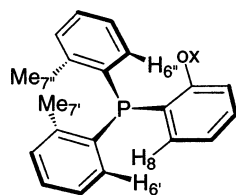
Fragment **A** for **5a**

The remaining aromatic protons were assigned via simple COSY and NOESY considerations, in that one can connect the individual protons within the three sets of four coupled spins via their ^{3}J(H,H) values and then position these with the help of NOEs: e.g., from the *o*-tolyl methyl groups. The two P(*o*-tolyl) rings can be distinguished in that one of these, in a pseudoaxial position, shows an NOE from the P(*o*-tolyl) methyl group, 7″, to the *tert*-butyl methyl groups as in fragment **B**.
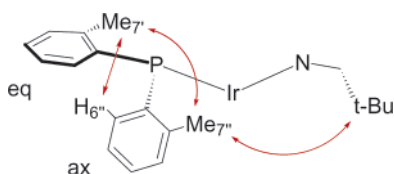
Fragment **B** for **5a**

This pseudoaxial ring is present in the solid state and appears to be a characteristic of PHOX-type ligands.[18,19] Two further sets of NOEs complete the conformational description of the P,N-chelate: (a) the two *o*-tolyl methyl groups reveal an interaction and (b) one P(o-tolyl) ring proton, H6″, sees the *o*-tolyl methyl, 7′, of the second equatorial P(*o*-tolyl) substituent.[20] Both of these contacts are also indicated in fragment **B**. Additional *inter*ligand NOEs, i.e., from methyl 7″ to an oxazoline methylene
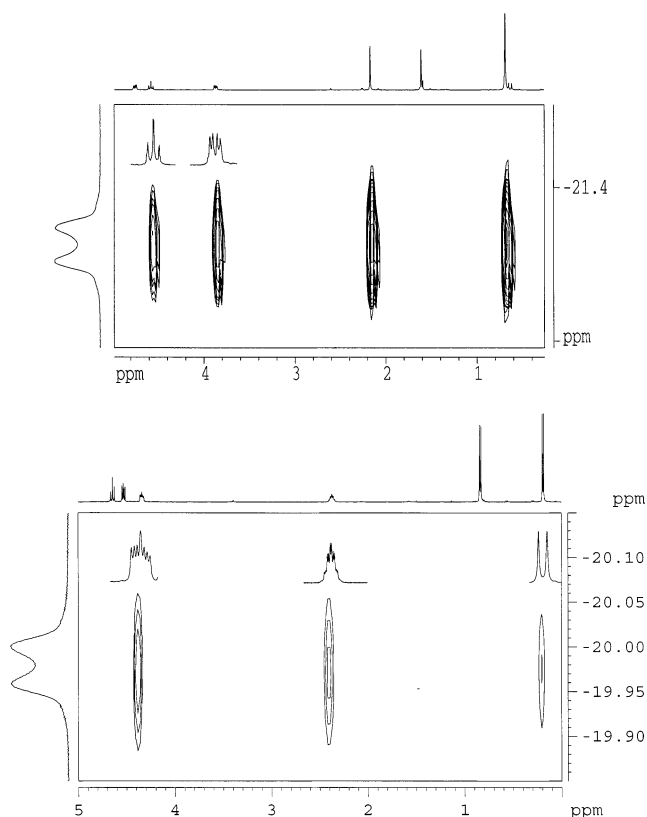

Figure 6. (a, top) Section of the NOESY spectrum for **5a** showing the four strong contacts to the terminal hydride ligand at δ −21.32. Two contacts derive from the *tert*-butyl and one P(*o*-tolyl) methyl group of one chelate ligand and the other two from mutually cis CHN and CHO protons of an oxazoline ring from a second chelating ligand. (b, bottom) Analogous interactions in the NOESY spectrum for **6** showing the three strong contacts to the terminal hydride ligand at δ −19.98. Two of these contacts derive from the isopropyl methine CH and one methyl group. The third arises from the CHN methine proton of an oxazoline ring from a second PHOX ligand.

proton, help to complete the solution picture, which is very similar to that found in the solid state.

With these assignments one can position the hydride ligands. All three hydride ligands reveal NOEs to their neighboring hydride donors, suggesting a pseudo-facial orientation of these three ligands. The bridging hydride shows one strong contact to the CHN methine proton and a weak interaction with the *tert*-butyl group. The two terminal hydrides reveal very different NOE contacts to the P,N-ligands. The resonance at δ −21.32 reveals four fairly strong contacts stemming from the *tert*-butyl and one P(*o*-tolyl) methyl group of one oxazoline and mutually cis CHN and CHO protons of a second oxazoline ring (see fragment **C** and Figure 6a). The remaining terminal hydride, found at δ −17.84, reveals one very strong NOE contact arising from an ortho tolyl arene proton of one P,N ligand and a P(*o*-tolyl) methyl

(18) (a) Selvakumar, K.; Valentini, M.; Worle, M.; Pregosin, P. S.; Albinati, A. *Organometallics* **1999**, *18*, 1207−1215. (b) Selvakumar, K.; Valentini, M.; Pregosin, P. S.; Albinati, A.; Eisentraeger, F. *Organometallics* **2000**, *19*, 1299−1307.
(19) Valentini, H.; Selvakumar, K.; Worle, M.; Pregosin, P. S. *J. Organomet. Chem.* **1999**, *587*, 244−251.
(20) Methyl 7′ is close to both H6″ and H8. Since these two resonances overlap, at δ 6.85, possibly the observed cross-peak involves both protons.

group of a second P,N ligand, as indicated in **D**. On the basis of these data we assign the relative positions of these hydrides as shown in **C** and **D**:
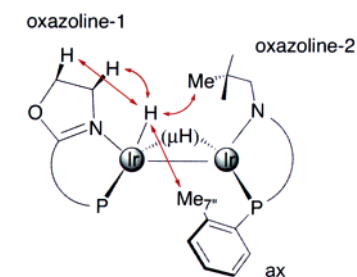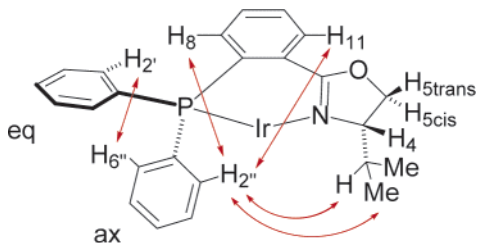

Relative position of hydride at −21.32
Fragment **C** for **5a**
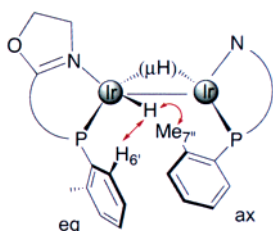
Relative position of hydride at −17.84
Fragment **D** for **5a**

Solution Structure for the Trinuclear Iridium Complex 6. The solution structure for **6** was also elucidated. The terminal hydride resonances are observed at δ −16.95 and −19.98 ppm, whereas the μ_3-hydride appears as a quartet at δ −6.15 ppm with the same ^2J(P,H) coupling constant, 46 Hz, found in **5a**.

Once again, the three hydride ligands are found to occupy a facial arrangement. As with **5a**, the μ_3-hydride is located on the nitrogen hemisphere of the Ir$_3$ triangle, as proven by NOE contacts to the i-Pr CH and C(4)−H methine protons. The NOE interactions between the hydride resonance at δ −19.98 and the isopropyl methyl groups of the oxazoline moiety are significantly stronger than from the second terminal hydride. Both terminal hydrides interact strongly with the ortho protons of the axial P-phenyl group, whereas the hydride at δ −16.95 is also close to the ortho protons of the equatorial P-phenyl group. The two P-phenyl rings can be distinguished in that one of the i-Pr Me groups, at δ 0.19, and the isopropyl methine reveal contacts with the axial 2″/6″ P-phenyl ortho protons. These (and other) NOEs are indicated in fragment **E**.
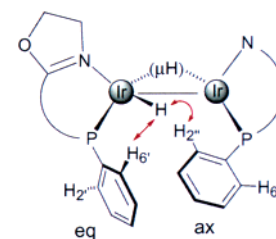

Fragment **E** for **6**

A detailed analysis of these NOE constraints permits an estimation of the hydride positions in **6** relative to

the chiral auxiliary, and in analogy with **5a** these are shown in fragments **F** and **G**.
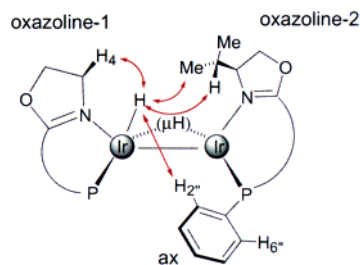
Relative position of hydride at −19.98
Fragment **F** for **6**

Relative position of hydride at −16.95
Fragment **G** for **6**

It is interesting that the hydride positions in both **5a** and **6** seem closely related. Indeed, a comparison of the NOE contacts for **5a** and **6b** (see parts a and b of Figure 6) reveals that the low-frequency terminal hydride is in a similar environment in both compounds. The estimated solution hydride positions for both **5a** and **6** are shown in the abbreviated structure **H**.
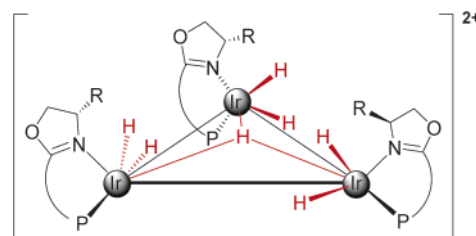
Fragment **H** for **5a** and **6**

Figure 7 shows how the different fragments **A**−**G** fit in a complete drawing of **5a** and **6**.

Since the NMR spectra for **6** were found to give sharper signals at 275 K compared to those at room temperature, variable-temperature ^{1}H and ^{31}P NMR spectra were recorded from 193 to 295 K (see Figure 8). A pronounced upfield shift of 0.57 ppm for the equatorial P-phenyl C(2′/6′)−H resonance was observed upon lowering the temperature from 295 to 193 K. At this temperature rotation around the various P−C bonds begin to slow[21] such that, most likely, the observed 0.57 ppm difference arises from a local anisotropic effect of the C6−C11 ring on the equatorial P-phenyl protons. The resonances of the terminal hydrides are closer together at low temperature: i.e., $\Delta\delta$ = 2.17 ppm at 193 K versus $\Delta\delta$ = 3.16 ppm at 295 K.

Electrospray mass spectra (ESI-MS) of the iridium hydride clusters **5b** and **6** in methanol were obtained.
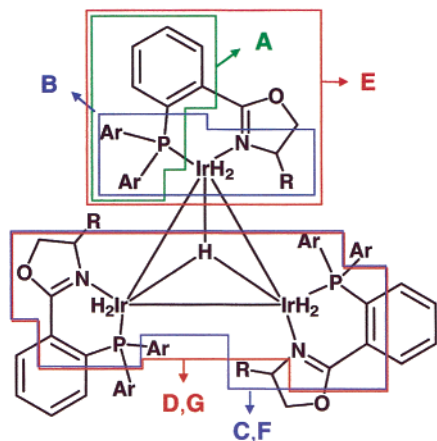
Figure 7. Complete structures for **5a** and **6**, showing the relative positions of the fragments described in the text.

We believe these to be the first applications of this method in Ir hydride cluster chemistry. An analysis of the data for **6** shows the presence of the dicationic cluster without anions as well as a monocationic species carrying one hexafluorophosphate anion. After a dilute solution of **6** was aged, a tetrameric species of composition $[Ir_4(\mathbf{2})_4(H)_{10}]^{2+}$ was detected.[22] When the complex was dissolved in dichloromethane, a significant amount of a dimeric iridium hydride species, probably of type $[Ir_2(\mathbf{2})_2(\mu_2\text{-}H)_3(H)_2]^+$, was formed in the ESI-MS at 200 °C capillary temperature.[23] Neither dinuclear nor tetranuclear Ir species have been observed in preparative experiments, to date.

Solution Structure for $[Ir(1,5\text{-}COD)(\mathbf{1})]PF_6$ (7). Given the recorded success of **1** as a chiral auxiliary, it seemed useful to characterize its chiral pocket in a second coordination environment. The solution structure of the pseudo-square-planar 1,5-COD complex **7** has been determined in a fashion analogous to that for **5a**. The interligand NOEs,[24] especially those involving the 1,5-COD olefin protons,[19,25] provide key data with respect to the structure of this compound.
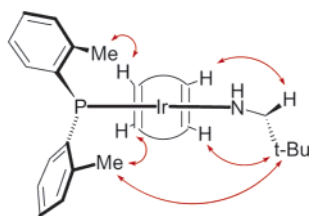
Fragment **I**, viewed from behind the complexed
1,5-COD, showing important NOE contacts

The 1,5-COD ligand in **7** affords four broad olefinic proton signals at δ 3.05, 3.48, 4.84, and 5.05. The $^{31}P,^1H$ correlation shows a cross-peak to only one olefinic proton at δ 4.84, indicating that this proton is pseudo-trans to

the P atom. From the same $^{31}P,^1H$ correlation it is possible to identify the coupled ortho (and meta) protons of the P(*o*-tolyl) moieties on the P atom.

The *tert*-butyl group of the oxazoline ring reveals an NOE with the olefinic proton at δ 4.84 and, as in **5a**, a second contact to one of the *o*-tolyl methyl groups. This implies that this 1,5-COD proton (which is known to be trans to the P atom) lies "below" the P–Ir–N plane (see **B**, above) and that, once again, there is a pseudoaxial P(*o*-tolyl) group. The second pseudo-trans 1,5-COD proton, at δ 5.05, can now be assigned via the COSY spectrum. This latter assignment is supported by a strong NOE from the olefinic resonance at δ 5.05 to the NCH methine absorption, thereby confirming its relative position.

Since one of the two remaining 1,5-COD protons, δ 3.48, shows a selective NOE to the assigned axial P(*o*-tolyl) methyl group, the remaining 1,5-COD olefinic protons are assigned. With these four 1,5-COD resonances, a $^1H–^{13}C$ HMQC experiment affords the corresponding four olefinic ^{13}C chemical shifts. As expected, these appear pairwise: δ 96.0 and 90.6 (trans to P) and δ 67.1 and 67.2 (trans to N). The > 20 ppm difference in chemical shift (cis to P relative to trans to P) arises from the known difference in trans influence between tertiary phosphine P and sp^2 N donors.[26–28]

The solution structure for **7** is related to that for **5**, in that they both reveal a chiral pocket involving one pseudoequatorial P-aryl substituent and one pseudoaxial (proximate to the oxazoline substituent) P-aryl group. However, the two P(*o*-tolyl) methyl groups do not reveal an NOE contact. Consequently, the orientation of the two *o*-tolyl groups may be slightly different than that found for **5a**. We cannot exclude some rotation of the 1,5-COD, relative to the P–Ir–N plane, as only one of the two olefinic protons is pseudo-trans to the P atom and shows a substantial coupling to the ^{31}P spin. NMR data for **7** are summarized in Table 5.

Reactivity Studies of 6. When complex **6** was treated with 90 bar of H_2 in CH_2Cl_2 for 2 h, no change in either the ^1H or ^{31}P NMR spectrum was observed. After 1 day, in the presence of 1 equiv of free PN ligand or NaH, again, the NMR spectra indicated the presence of unchanged **6**. Catalytic hydrogenation reactions with three alkenes commonly used in previous catalytic studies[7] were attempted under 50 atm of hydrogen gas in CH_2Cl_2 for 2 h. For all three alkenes tested (*trans*-α-methylstilbene, 3-phenyl-but-2-enoic acid ethyl ester,

(21) (a) Empsall, H. D.; Hyde, E. M.; Shaw, B. L. *J. Chem. Soc., Dalton Trans.* **1975**, 1690–1696. (b) Empsall, H. D.; Hyde, E. M.; Shaw, B. L.; Jones, C. E.; Shaw, B. L. *J. Chem. Soc., Dalton Trans.* **1974**, 1980–1985. (c) Mann, B. E.; Masters, C.; Shaw, B. L.; Stainbank, R. E. *J. Chem. Soc., Chem. Commun.* **1971**, 1103–1104.

(22) Upon standing of the diluted solution, the tetranuclear complex $[Ir_4(PN)_4(H)_{10}]^{2+} = C_{96}H_{106}N_4O_4Ir_4P_4$ was formed, and its formula could be proven by HR-ESI-MS: *m/e* calcd 1136.282 36, found 1136.283 39 for $[M\{3 \times {}^{193}Ir, 1 \times {}^{191}Ir\} - 2PF_6]^{2+}$.

(23) $[Ir_2(PN)_2(H)_5]^+ = C_{48}H_{53}N_2O_2P_2Ir_2$: *m/e* 851.9 ([trimer − 2PF_6]^{2+}, 6%), 1135.4 ([dimer − PF_6]^+, 100%).

(24) (a) Trabesinger, G.; Albinati, A.; Feiken, N.; Kunz, R. W.; Pregosin, P. S.; Tschoerner, M. *J. Am. Chem. Soc.* **1997**, *119*, 6315–6323. (b) Pregosin, P. S.; Trabesinger, G. *J. Chem. Soc., Dalton Trans.* **1998**, 727–734. (c) Pregosin, P. S. In *Advances in BioChirality*; Palyi, G., Zucchi, C., Caglioti, L., Eds.; Elsevier SA: 1999; pp 335–345. (d) Drago, D.; Pregosin, P. S.; Razavi, A. *Organometallics* **2000**, *19*, 1802–1805. (e) Pregosin, P. S.; Valentini, M. *Enantiomer* **1999**, *4*, 529–539.

(25) (a) Feiken, N.; Pregosin, P.; Trabesinger, G. *Organometallics* **1998**, *17*, 4510–4518. (b) Albinati, A.; Eckert, J.; Pregosin, P. S.; Rüegger, H.; Salzmann, R.; Stössel, C. *Organometallics* **1997**, *16*, 579–590.

(26) Åkermark, B.; Krakenberger, B.; Hansson, S.; Vitagliano, A. *Organometallics* **1987**, *6*, 620.

(27) (a) Dotta, P.; Magistrato, A.; Röthlisberger, U.; Pregosin, P. S.; Albinati, A. *Organometallics* **2002**, *21*, 3033–3041. (b) Dotta, P.; Anil Kumar, P. G.; Pregosin, P. S. *Magn. Reson. Chem.* **2002**, *40*, 653–658.

(28) Woo, T. K.; Pioda, G.; Röthlisberger, U.; Togni, A. *Organometallics* **2000**, *19*, 2144–2152.
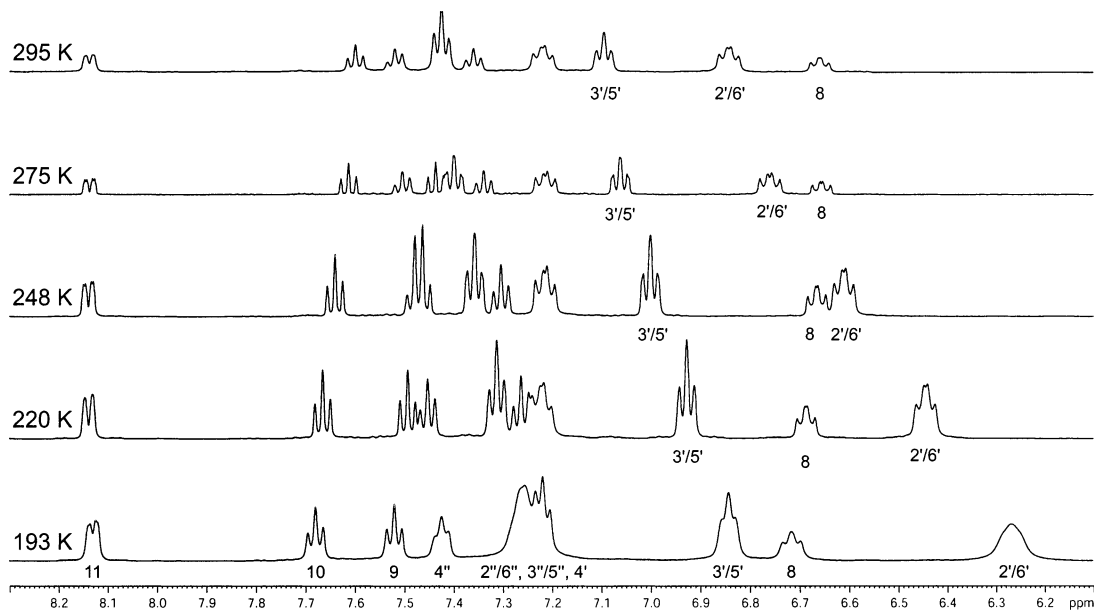
Figure 8. Variable-temperature ^{1}H NMR spectra of **6** in CD_2Cl_2 at 500 MHz. The change in the aromatic region stems primarily from the ortho and meta protons 2′/6′ and 3′/5′.

Table 3. ^{1}H NMR Data for 5a and 6

position	5a^a	6^b
R		
Me	0.67 (s)	0.19 (d, 7 Hz)
		0.83 (d, 8 Hz)
C*H*		2.37 (d sept, 3, 7 Hz)
4	3.84 (dd, 10, 4 Hz)	4.34 (ddd, 3, 6, 10 Hz)
5		
cis to R	4.72 (dd, 10, 4 Hz)	4.52 (dd, 6, 10 Hz)
trans to R	4.54 (dd,^{c} 10 Hz)	4.64 (dd^c, 10 Hz)
8	6.84 (m)	6.66 (dd, J_{HH} = 8 Hz, J_{PH} = 10 Hz)
9	7.37 (dd,^{c} 7 Hz)	7.44 (dd,^{c} 8 Hz)
10	7.43 (dd,^{c} 8 Hz)	7.61 (dd,^{c} 8 Hz)
11	8.14 (dd, 7, 2 Hz)	8.14 (dd, J_{HH} = 8 Hz, J_{PH} = 2 Hz)
equatorial *o*-Tol/Ph		
2′		6.76 (dd, 8, 12 Hz)
3′	7.14 (m)	7.06 (dd,^{c} 8 Hz)
4′	7.26 (dd,^{c} 8 Hz)	7.34 (dd,^{c} 7 Hz)
5′	6.26 (dd,^{c} 7 Hz)	7.06 (dd,^{c} 8 Hz)
6′	7.98 (dd,^{c} 8 Hz)	6.76 (dd, 8, 12 Hz)
7′	1.58 (s)	
axial *o*-Tol/Ph		
2″		7.21 (dd, J_{HH} = 8 Hz, J_{PH} = 12 Hz)
3″	7.47 (bs)	7.40 (dd,^{c} 8 Hz)
4″	7.48 (m)	7.50 (dd,^{c} 7 Hz)
5″	7.16 (m)	7.40 (dd,^{c} 8 Hz)
6″	6.82 (m)	7.21 (dd, J_{HH} = 8 Hz, J_{PH} = 12 Hz)
7″	2.14 (s)	
hydrides		
bridging	−7.07 (q, $^2J_{PH}$ = 46 Hz)	−6.15 (q, $^2J_{PH}$ = 46 Hz)
terminal	−17.84 (s)	−16.95 (d, $^2J_{PH}$ = 5 Hz)
	−21.32 (d, $^2J_{PH}$ = 23 Hz)	−19.98 (d, $^2J_{PH}$ = 21 Hz)

^{a} 400 MHz. ^{b} 500 MHz. ^{c} Similar ^3J values. ^4J not resolved.

and 1-methoxy-4-(1-methylenepropyl)benzene) there was no conversion. Obviously, these trinuclear iridium compounds are relatively robust and do not readily react to produce the mononuclear iridium hydride species which might be expected to function as hydrogenation catalysts. These observations on reactivity (or the lack

thereof) support the hypothesis that in situ trimerization to form, e.g., **5b** or **6** would be accompanied by loss of catalytic activity.
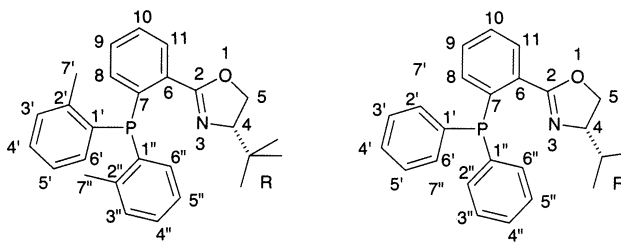
Experimental Section

NMR spectra for **5** and **6** were recorded on a Bruker Avance 400 and 500 MHz NMR spectrometer equipped with inverse (400 MHz) and BBO broadband (500 MHz) probeheads. IR spectra were recorded on a Perkin-Elmer 1600 series spectrometer. High-resolution ESI (electrospray ionization) mass spectra were measured with a Bruker FTMS 4.7 T Bio APEXII spectrometer. Low-resolution ESI mass spectra were also measured with a Finnigan MAT LCQ octapole mass spectrometer. The elemental analysis of **6** was done by the microanalytical laboratory of the University of Basel, and those of **5a** and **5b** were performed by a similar laboratory at the ETH Zürich.

Synthesis of [Ir$_3$(μ_3-H)H$_6$(1)$_3$](PF$_6$)(OTf) (5a). A solution of [Ir(COD)(**1**)]OTf (90 mg, 0.10 mmol) and KPF$_6$ (380 mg, 2 mmol) in 1 mL of dry MeOH was stirred under 1 atm of H$_2$ for 16 h. After ca. 2 h, the product precipitated as a yellow, microcrystalline powder. The solid was collected via filtration and washed with Et$_2$O. The crude product was recrystallized from CH$_2$Cl$_2$/Et$_2$O. Yield: 52 mg, 75%. The product is soluble in CH$_2$Cl$_2$ and partially soluble in MeOH. See Tables 3 and 4 for NMR data. Anal. Calcd for C$_{82}$H$_{97}$Ir$_3$F$_9$N$_3$O$_6$P$_4$S: C, 46.36; H, 4.60; N, 1.98. Found: C, 46.21; H, 4.82; N, 1.87.

Synthesis of [Ir$_3$(μ_3-H)H$_6$(1)$_3$](OTf)$_2$ (5b). A solution of [Ir-(COD)(**1**)]OTf (155 mg, 0.17 mmol) in 1 mL of MeOH was stirred under 1 atm of H$_2$ for 16 h. After ca. 2 h, the product precipitated as a yellow, microcrystalline powder. The product was collected via filtration and washed with Et$_2$O. Yield: 98 mg, 81%. Compound **5b** is soluble in CH$_2$Cl$_2$ and partially soluble in MeOH. Anal. Calcd for C$_{83}$H$_{97}$Ir$_3$F$_6$N$_3$O$_9$P$_3$S$_2$: C, 46.84; H, 4.59; N, 1.97. Found: C, 46.70; H, 5.08; N, 1.92; ESI-MS (CH$_2$Cl$_2$, m/e): 915.5 ([M{2 × ^{193}Ir, 1 × ^{191}Ir} − 2PF$_6$]$^{2+}$, 100%). IR (cm^{-1}): $\tilde{\nu}$ 3071 w; 2956 m ($\nu_{C−H}$); 2931 m ($\nu_{C−H}$); 2231 br, m (H$^−$); 1784 br, m (H$^−$); 1606 s. ^{31}P NMR (162.0 MHz): 8.8 (s). ^{19}F NMR (376.3 MHz): −79.3 (s).

Synthesis of [Ir$_3$(μ_3-H)H$_6$(2)$_3$](PF$_6$)$_2$ (6). A suspension of finely ground [Ir(COD)(**2**)]PF$_6$ (200 mg, 0.244 mmol) in 7 mL of dry MeOH was stirred under 1 atm of H$_2$ for 2 h. The initially red slurry dissolved after 5 min to afford an orange solution. After 10 min, the product began to precipitate as a

Table 4. $^{13}C\{^{1}H\}$, $^{31}P\{^{1}H\}$, and $^{19}F\{^{1}H\}$ NMR Data for 5a and 6
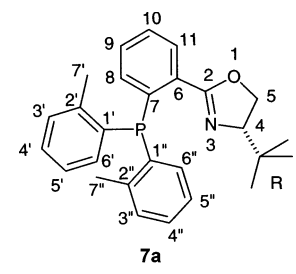
position	5a	6
	^{13}C NMR^a	
R		
Me	26.9 (s)	12.2 (s)
		18.5 (s)
CH	35.6 (s)	28.9 (s)
2	168.4 (s)	163.1 (s)
4	84.0 (s)	79.3 (s)
5	71.2 (s)	68.1 (s)
6	129.0 (m)	129.0 (m)
7	128.4 (m)	128.0 (m)
8	132.1 (bs)	131.7 (bs)
9	134.8 (s)	133.4 (s)
10	132.2 (s)	132.3 (s)
11	133.6 (m)	131.9 (bs)
equatorial o-Tol/Ph		
1′	123.0 (m)	129.9 (d, $^1J_{PC}$ = 70 Hz)
2′	142.2 (m)	132.4 (m)
3′	133.8 (m)	128.9 (m)
4′	133.1 (bs)	132.2 (m)
5′	127.7 (m)	128.9 (m)
6′	136.9 (m)	132.4 (m)
7′	22.9 (s)	
axial o-Tol/Ph		
1″	132.2 (m)	130.7 (d, $^1J_{PC}$ = 71 Hz)
2″	140.5 (m)	132.7 (m)
3″	133.1 (bs)	129.1 (m)
4″	132.9 (s)	132.5 (s)
5″	127.4 (m)	129.1 (m)
6″	131.5 (m)	132.7 (m)
7″	23.4 (m)	
	^{31}P NMR (202.4 MHz)	
	8.25 (s)	14.8 (s)
	−143.2	−144.7
	^{19}F NMR (376.3 MHz)	
	−73.9 (d, $^2J_{PF}$ = 711 Hz)	−74.5 (d, $^1J_{PF}$ = 711 Hz)
	−79.3 (s)	

^{a} 75.4 MHz for **5a** and 125.8 MHz for **6**.

Table 5. NMR Data^a for 7a

7a

position	^1H	^{13}C
4	4.05 (d, $^3J_{HH}$ = 9.4)	74.9 (s)
5	4.52 (dd, $^3J_{HH}$ = 9.5, $^3J_{HH}$ = 9.4)	70.6 (s)
5	4.67 (br d, $^3J_{HH}$ = 9.4)	70.6 (s)
8	7.82 (dd, $^3J_{HH}$ = 7.3, $^3J_{HH}$ = 7.2)	132.5 (s)
9	7.70 (dd, $^3J_{HH}$ = 7.2, $^3J_{HH}$ = 7.0)	134.4
10	7.29 (dd, $^3J_{PH}$ = 7.5, $^3J_{HH}$ = 7.1)	134.6 (d, $^2J_{PC}$ = 9.3)
11	8.37 (dd, $^3J_{HH}$ = 7.3, $^4J_{HH}$ = 3.8)	134.2 (s)
R		34.5 (s) quat C
R	0.69 (s)	25.2 (s) t-Bu Me
equatorial tol ring		
1′		120.0 (d, $^1J_{PC}$ = 52.6)
2′		141.8 (d, $^2J_{PC}$ = 26.8)
3′	7.44 (d, $^3J_{HH}$ = 7.3)	133.0 (s)
4′	7.52 (m)	132.3 (s)
5′	7.29 (br $^3J_{HH}$ = 7.5, $^3J_{HH}$ = 7.5)	127.3 (s)
6″	6.94 (dd, $^3J_{PH}$ = 9.7, $^3J_{HH}$ = 8.3)	134.1 (d, $^2J_{PC}$ = 9.0)
7′	2.40 (s)	25.2 (s)
axial tol ring		
1″		130.5 (d, $^1J_{PC}$ = 56.0)
2″		143.5 (br s)
3″	7.53 (m)	133.1 (s)
4″	7.47 (m)	132.6 (m)
5″	7.11 (d,d, $^3J_{HH}$ = 8.2, $^3J_{HH}$ = 7.0)	127.4 (s)
6″	6.57 (d,d, $^3J_{PH}$ = 9.2, $^3J_{HH}$ = 8.2)	134.0 (d, $^2J_{PC}$ = 9.2)
7″	3.14 (s)	24.9 (s)
1,5-COD olefinic^b	5.05 (br)	96.0 (d, $^2J_{PC}$ = 12.4) trans to P
	4.84 (br)	90.6 (d, $^2J_{PC}$ = 14.1) trans to P
	3.48 (br)^c	67.2 (br) trans to N
	3.05 (br)	67.1 (br) trans to N

^{a} Chemical shifts are in ppm and J values in Hz. ^{b} Aliphatic 1,5-COD resonances ^1H (^{13}C): 2.11 (m), 1.54 (m) (28.4), 2.50 (35.9), 2.12 (m), 1.66 (25.3), 2.44 (33.1). See text for details. ^{c} This olefin proton shows an NOE to the pseudoaxial P(o-tolyl) methyl group. Therefore, it is assigned as being on the same side of the P−Ir−N plane.

yellow, microcrystalline powder. The solid was collected via filtration and washed with dry MeOH and dry Et_2O. Yield: 100 mg, 62%. The product is soluble in dichloromethane and partially soluble in MeOH. An analogous reaction with [Ir(o-Tol$_2$;t-Bu-PHOX)(COD)]PF$_6$ leads to **5c**. Anal. Calcd for $C_{72}H_{79}$-Ir$_3$F$_{12}$N$_3$O$_3$P$_5$: C, 43.37; H, 3.99; N, 2.11. Found: C, 42.64; H, 4.14; N, 1.91. Mp: 270 °C dec. ESI-MS (MeOH, 5 V capillary voltage, m/e): 851.71 ([M{2 × ^{193}Ir, 1 × ^{191}Ir} − 2PF$_6$]$^{2+}$, 100%); 1848.40 (M{2 × ^{193}Ir, 1 × ^{191}Ir} − PF$_6$]$^+$, 35%).[23] HR-ESI-MS (MeOH, m/e): calcd 851.709 38, found 851.708 95 for [M{2 × ^{193}Ir, 1 × ^{191}Ir}− 2PF$_6$]$^{2+}$.[22] IR (KBr, cm^{-1}): $\tilde{\nu}$ 3060 w; 2961 m (ν_{C-H}); 2190 br, m (H$^-$); 1734 br, w (H$^-$); 1622 s; 1483 s; 1437 s; 1380 s; 1244 m; 1121 m; 1100 s; 841 vs; 693 s; 558 vs; 516 m cm^{-1}.

Crystallography. Table 6 gives crystallographic data for **5a** and **6**.

Structural Study of [Ir$_3$(μ_3-H)H$_6$(1)$_3$](PF$_6$)(CF$_3$SO$_3$) (5a). Yellow crystals of **5a** suitable for X-ray diffraction were obtained from CH_2Cl_2/Et$_2$O. For the data collection, a small

prismatic single crystal was mounted on a glass fiber, at a random orientation, on a Bruker APEX CCD diffractometer and cooled, with a cold nitrogen stream, to 113(2) K. The space group was determined from the systematic absences, while the cell constants were refined, at the end of the data collection, using the data reduction software SAINT.[29] Data were collected by using ω scans in steps of 0.3°; a list of experimental conditions for the data collection is given in Supplementary Table S1 (Supporting Information). The collected intensities were corrected for Lorentz and polarization factors[29] and empirically for absorption using the SADABS program.[30]

(29) SAINT: SAX Area Detector Integration; Siemens Analytical Instrumentation, Madison, WI, 1996.
(30) Sheldrick, G. M. SADABS; Universität Göttingen, Göttingen, Germany, 1999.

**Table 6. Crystallographic Data for
[Ir$_3$(μ_3-H)H$_6$(1)$_3$](PF$_6$)(CF$_3$SO$_3$) (5a) and
[Ir$_3$(μ_3-H)H$_6$(2)$_3$](PF$_6$)$_2$ (6)**

	5a	6
formula	C$_{82}$H$_{91}$F$_9$Ir$_3$N$_3$O$_6$P$_4$S	C$_{72}$H$_{72}$F$_{12}$Ir$_3$N$_3$O$_3$P$_5$
mol wt	2118.12	1993.92
data collecn T, K	113(2)	293
diffractometer	Bruker APEX	KappaCCD
cryst syst	orthorhombic	orthorhombic
space group (No.)	$P2_12_12$ (18)	$P2_12_12_1$ (19)
a, Å	25.203 (11)	13.7272 (5)
b, Å	29.901 (9)	21.4699 (6)
c, Å	12.045 (5)	27.2560 (12)
V, Å^3	9077 (6)	8032.9 (5)
Z	4	4
ρ_{calcd}, g cm^{-3}	1.550	1.643
μ, cm^{-1}	45.47	51.29
radiation	Mo Kα (graphite monochrom. λ = 0.710 73 Å)	
θ range, deg	$1.58 < \theta < 27.50$	$3.06 < \theta < 29.06$
no. of indep data	19113	21249
no. of obsd rflns (n_o) ($|F_o|^2 > 2.0\sigma(|F|^2)$)	15393	15400
no. of params refined (n_v)	977	1012
R1 (obsd rflns)^a	0.0579	0.0515
wR2 (obsd rflns)^b	0.0748	0.0467
GOF^c	0.922	1.0515

^{a} R1 = $\sum(|F_o - (1/k)F_c|)/\sum|F_o|$. ^{b} wR2 = $[\sum w(F_o^2 - (1/k)F_c^2)^2/\sum w|F_o^2|^2]$. ^{c} GOF = $[\sum w(F_o^2 - (1/k)F_c^2)^2/(n_o - n_v)]^{1/2}$.

Selected crystallographic and other relevant data are listed in Table 6 and in Supplementary Table S1. The standard deviations on intensities were calculated in term of statistics alone, while those on F_o^2 were calculated as shown in Table 6 and S1.

The structure was solved by Patterson and Fourier methods and refined by full-matrix least squares,[31] minimizing the function $[\sum w(F_o^2 - (1/k)F_c^2)^2]$ and using anisotropic displacement parameters for all atoms. No extinction correction was deemed necessary. Toward the end of the refinement the Fourier difference map showed a peak, in a position consistent with the presence of a triply bridging hydride, in accordance with the NMR data. Therefore, this hydride position was refined in the final least-squares cycles, without constraints, using an isotropic temperature factor. The refined positional parameters gave an acceptable geometry, although the associated large esd's prevent a detailed discussion of the bridging geometry. Upon convergence (see Supplementary Table S1) the final Fourier difference map showed no significant peaks.

The contribution of the hydrogen atoms, in their calculated positions (C–H = 0.95 Å, B(H) = 1.3/1.5[B(C$_{bonded}$)] (Å^2)), was included in the refinement using a riding model. Refining Flack's parameter[32] tested the handedness of the structure.

All calculations were carried out by using the PC version of the SHELX-97 and ORTEP programs.[31] The scattering factors used, corrected for the real and imaginary parts of the anomalous dispersion, were taken from the literature.[33]

X-ray Crystal Structure Analysis of 6. Orange crystals of **6** were obtained from CH$_2$Cl$_2$/Et$_2$O. A crystal of size 0.32 × 0.20 × 0.04 mm was mounted at random orientation on a glass fiber, and the data were collected on a KappaCCD four-circle diffractometer at 293 K. The space group was determined from the systematic absences using the software suite Collect (Nonius BV, 2002). Integration of frames was done with EvalCCD (Bruker Nonius BV, 2002). The collected intensities were corrected empirically for absorption using the SORTAV program.[34] Selected crystallographic and other relevant data are listed in Table 6.

The structure was solved by direct methods with SIR92[35] and refined with CRYSTALS[36] by full-matrix least squares by minimizing the function $[\sum w(F_o - (1/k)F_c)^2]$ and using anisotropic displacement parameters for all atoms. No extinction correction was deemed necessary. A Chebychev polynomial with four parameters was applied as a weighting scheme.[37] Restraints were applied to the disordered hexafluorophosphate anions.

The contribution of the hydrogen atoms, in their calculated positions (C–H = 0.95 Å, B(H) = 1.3/1.5[B(C$_{bonded}$)] (Å^2)), was included in the refinement using a riding model. The hydrido ligands bound to iridium could not be located. Refining Flack's parameter[32] tested the handedness of the structure. Upon convergence, the final Fourier difference map showed no significant peaks. The scattering factors used, corrected for the real and imaginary parts of the anomalous dispersion, were taken from the literature.[33]

For the generation of graphics, ORTEP-3 for Windows Version 1.073 was used.[31b] Crystallographic data (excluding structure factors) for **6** have been deposited with the Cambridge Crystallographic Data Centre as Deposition No. CCDC-192567. Copies of the data can be obtained, free of charge, on application to the CCDC, 12 Union Road, Cambridge CB2 1EZ, U.K. (fax, +44 (1223) 336 033; e-mail, deposit@ccdc.cam.ac.uk).

Supporting Information Available: Text giving experimental details and a full listing of crystallographic data for compounds **5a** and **6**, including tables of positional and isotropic equivalent displacement parameters, calculated positions of the hydrogen atoms, anisotropic displacement parameters, and bond distances and angles and ORTEP figures showing the full numbering schemes. This material is available free of charge via the Internet at http://pubs.acs.org.

OM020805A

(31) (a) Sheldrick, G. M. SHELX-97. Structure Solution and Refinement Package; Universität Göttingen, Göttingen, Germany, 1997. (b) Farrugia, L. J. *J. Appl. Crystallogr.* **1997**, *30*, 565.
(32) Flack, H. D. *Acta Crystallogr., Sect. A* **1983**, *A39*, 876.
(33) *International Tables for X-ray Crystallography*; Wilson, A. J. C., Ed.; Kluwer Academic: Dordrecht, The Netherlands, 1992; Vol. C.
(34) Blessing, R. H. *Acta Crystallogr.* **1995**, *A51*, 33–38.
(35) Altomare, A.; Cascarano, G.; Giacovazzo, C.; Gualgliardi, A.; Burla, M. C.; Polidori, G.; Camalli, M. *J. Appl. Crystallogr.* **1994**, *27*, 435.
(36) Watkin, D. J.; Prout, C. K.; Carruthers, J. R.; Betteridge, P. W.; Cooper, R. I. CRYSTALS Issue 11.6; Chemical Crystallography Laboratory, University of Oxford, Oxford, U.K., 2001.
(37) Carruthers, J. R.; Watkin, D. J. *Acta Crystallogr., Sect. A* **1979**, *35*, 698.